

# Discovering Dynamic Symbolic Policies with Genetic Programming

Sigur de Vries<sup>1\*</sup>, Sander Keemink<sup>1</sup>, and Marcel van Gerven<sup>1</sup>

<sup>1</sup>Department of Machine Learning and Neural Computing, Donders Institute for Brain, Cognition and Behaviour, Radboud University, Nijmegen, the Netherlands

\*sigur.devries@ru.nl

## Abstract

Artificial intelligence (AI) techniques are increasingly being applied to solve control problems. However, control systems developed in AI are often black-box methods, in that it is not clear how and why they generate their outputs. A lack of transparency can be problematic for control tasks in particular, because it complicates the identification of biases or errors, which in turn negatively influences the user's confidence in the system. To improve the interpretability and transparency in control systems, the black-box structure can be replaced with white-box symbolic policies described by mathematical expressions. Genetic programming offers a gradient-free method to optimise the structure of non-differentiable mathematical expressions. In this paper, we show that genetic programming can be used to discover symbolic control systems. This is achieved by learning a symbolic representation of a function that transforms observations into control signals. We consider both systems that implement static control policies without memory and systems that implement dynamic memory-based control policies. In case of the latter, the discovered function becomes the state equation of a differential equation, which allows for evidence integration. Our results show that symbolic policies are discovered that perform comparably with black-box policies on a variety of control tasks. Furthermore, the additional value of the memory capacity in the dynamic policies is demonstrated on experiments where static policies fall short. Overall, we demonstrate that white-box symbolic policies can be optimised with genetic programming, while offering interpretability and transparency that lacks in black-box models.

## 1 Introduction

Many problems in our increasingly complex society can be viewed as control problems, where the goal is to make optimal decisions in real time such as to regulate the behaviour of the controlled system, ranging from smart infrastructure systems to healthcare systems [3]. In recent years, there have been many successful applications of artificial intelligence (AI) to control problems, offering automated solutions to regulate complex non-linear processes. While the employed control algorithms achieve high performance, they usually require the use of black-box models such as neural networks [1]. Such black-box models often allow for highly general computations, but lack interpretability of their functioning, making it difficult to understand the computed decisions and actions [25]. Transparency is particularly important in control systems, because it aids in identification of biases, fault detection and improvement and could therefore raise confidence of users in the system's reliability [42].

In contrast to black-box models, white-box models allow for easy inspection of their internal mechanisms [1]. However, white-box models show an accuracy-interpretability trade-off and there are currently no general training methods to produce white-box approaches that can compete with black-box approaches in terms of efficiency and accuracy [25, 28]. Most white-box approaches opt for post-training model distillation to produce a transparent model that learns the input-output mapping of a black-box model [12]. Disadvantages of model distillation are that it requires a two-phase learning process and information loss could occur in the distillation phase [31]. Therefore, it may be more desirable to learn white-box models from the start. When training an inherently white-box model, interpretability of decisions already occurs at intermediate stages, showing transparent learning, and outputs are directly dependent on explainable features [31].

One way to learn white-box control systems is to discover symbolic policies [24, 12]. Symbolic policy learning is a relatively new field, but it is closely related to symbolic regression [6]. Most applications of symbolic regression focus on discovering the equations that govern unknown dynamics [8, 32, 19, 34, 29]. In contrast, symbolic policy learning

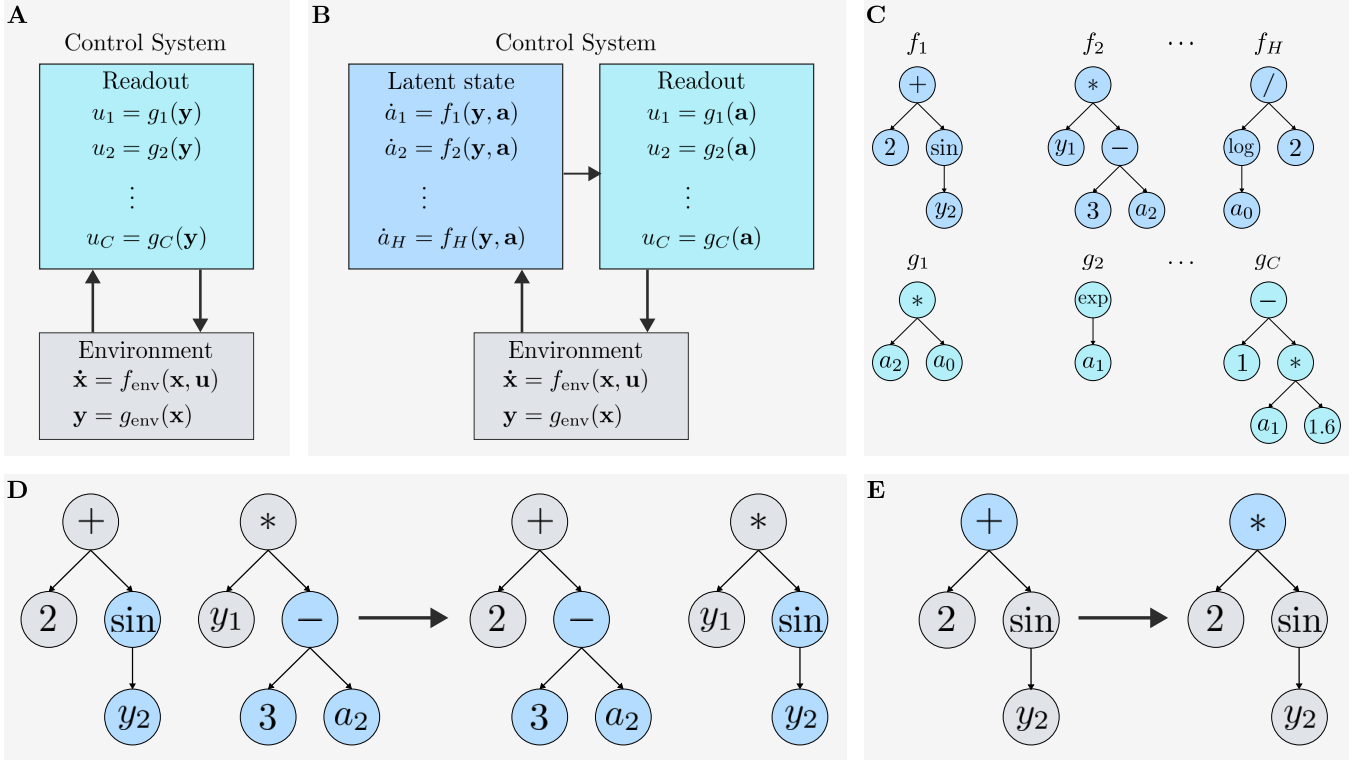


Figure 1: **General overview of the setup of the study.** (A) The feedback loop of an environment coupled with a control system that implements a static policy.  $C$  represents the number of control signals required to interact with the environment. For every function  $g_j$  a tree is optimised. (B) The control system is extended to include a latent state to implement a dynamic policy.  $H$  represents the number of units in the latent state. (C) An example representation of how a dynamic symbolic policy is represented by a set of parse trees. A tree is learned for every latent state and output signal. The functions  $f_i$  and  $g_j$  match the control system’s structure defined in panel B. (D) In genetic programming, crossover is applied to a pair of parents and produces two offspring individuals. The colored subtrees are interchanged between the two trees. (E) In genetic programming, mutation changes one individual and results in a single offspring. In this example, the colored node is a function node that is changed to a different type of function node.

focuses on discovering the control laws that can optimally control the system it interacts with. Symbolic policies are described by symbolic expressions, consisting of mathematical operators and relevant state variables. Similar to symbolic regression [6], symbolic policy learning does not require a predefined model structure, therefore it is less affected by human bias or knowledge gaps compared to other data-driven approaches. Besides being interpretable, symbolic policies have other advantages such as that the policies may capture rules that generalise better to other settings due to the bias-variance trade-off, and learned equations tend to be more efficient than neural networks in terms of parameter count.

Nonetheless, there are several challenges that make it difficult to learn symbolic expressions. The search space of combinations of operators and variables is extremely large and the structure of a mathematical expressions is non-differentiable, meaning that nonlinear function approximators such as neural networks cannot be easily applied. Furthermore, current methods of symbolic policy learning focus on static policies, and can rarely scale to multiple control dimensions. Dealing with partial observability and varying environment settings are however big challenges in control problems, which requires a policy to have memory to accomplish its goals [15]. Therefore it is important to learn dynamic symbolic policies to improve the robustness of the policies.

To address these challenges, we introduce a new evolutionary approach to optimise high-performing white-box models to solve control problems. Evolutionary algorithms have achieved many successes in control and reinforcement learning tasks. Work in [33] and [37] showed that genetic algorithms and evolution strategies are powerful alternatives

for gradient-based approaches for optimisation of weights of neural networks. NEAT [36] extends genetic algorithms by evolving neural network architectures from scratch while learning the weights simultaneously. In contrast to these methods, we propose to use genetic programming to learn the structure of dynamical systems that directly implement effective control policies. To this end, we embrace genetic programming (GP). This is an evolutionary approach which offers a gradient-free method to learn computer programs [23]. Therefore, GP can also be used to discover symbolic policies for control problems [16].

A GP approach is developed to learn both static and dynamic symbolic policies to solve control problems. Formally, static policies learn a fixed mapping from observations to control outputs (Figure 1A). However, this approach falls short when the environment is volatile (changes across time) or partially observable (providing limited information about the state of the environment). In this case, we are in need of dynamic control systems that integrate past observations to make optimal decisions (Figure 1B). In the dynamic case, the GP learns a symbolic representation of a state equation, describing the flow of a differential equation that takes observations as input and generates controls as output. Here, the latent state of the underlying differential equations functions as a memory system to capture long term dependencies in the data, which could improve the policy’s robustness and generalisability [15]. This is similar to the use of neural differential equations to estimate parameterized dynamical systems. However, in contrast to neural differential equations we learn a symbolic, interpretable, representation of the state equation that implements the policy.

When symbolic policies with higher dimensionality or with a latent space are optimised, the trees have to be evolved simultaneously, which complicates optimisation of the trees due to the large search space. Our method is extended to improve the efficiency of traversing the search space to discover high-performing static and dynamic symbolic policies consisting of multiple trees. Hence, in the case of dynamic policies, GP learns a symbolic expression for every dimension of the latent state and the readout function (Figure 1C).

Using this approach, symbolic policies are discovered for benchmark linear and non-linear environments as well as a simulation of an industrial problem. Dynamic policies are successfully evolved in environments with partial observability and varying parameter settings whereas static policies obtain limited performance in these settings. High-performing symbolic policies are still discovered when the control dimension increases, showing that our method is scalable. Furthermore, we find that the evolved symbolic policies obtain comparable performance as the black-box baseline, given by neural differential equations [9]. The key contribution of our work is a method for discovering interpretable high-performing static and dynamic symbolic policies with GP without requiring human expertise.

## 2 Methods

The goal of this paper is to find static and dynamic symbolic policies that obtain high performance in control problems. The general setup in our experiments contains an environment coupled with a static policy (Figure 1A) and a dynamic policy (Figure 1B), which is explained in more detail in this section. Afterwards, the specifics of the GP algorithm and how we extended GP to learn multiple trees efficiently are described. In subsequent subsections the baselines and experiments we performed are detailed. The code including genetic programming implementation, environments and baselines can be found at: <https://github.com/sdevries0/MultiTreeGP>.

### 2.1 Environment model

To evaluate a symbolic policy proposed by GP, a coupled system consisting of the policy and an environment is simulated, as described in Figure 1A and Figure 1B. The environment is modeled by a state  $\mathbf{x} \in \mathbb{R}^N$ , following the dynamics of a stochastic differential equation

$$d\mathbf{x} = f_{\text{env}}(\mathbf{x}, \mathbf{u}) dt + \mathbf{V}d\mathbf{w} \quad (1)$$

where  $\mathbf{u} \in \mathbb{R}^C$  is the control input,  $f_{\text{env}}$  is the environment’s state equation,  $\mathbf{w} \in \mathbb{R}^K$  is a multivariate Wiener process and  $\mathbf{V} \in \mathbb{R}^{N \times K}$  determines how the process noise influences the dynamics. The policies are evaluated on a batch of trajectories, with a batch size of 32. In every trajectory, the initial conditions is randomly sampled, and if applicable a target state and environment parameters are sampled.

The controller does not have direct access to  $\mathbf{x}$ , but instead receives observations  $\mathbf{y} \in \mathbb{R}^M$  about the state  $\mathbf{x}$ , determined by function  $g_{\text{env}}$  and possibly corrupted by noise. In our experiments, the noisy observations are generated by

$$\mathbf{y} = \mathbf{D}\mathbf{x} + \epsilon \quad (2)$$

where  $\mathbf{D} \in \mathbb{R}^{M \times N}$  is a readout matrix and  $\epsilon \sim \mathcal{N}(\mathbf{0}, \Sigma)$  is Gaussian observation noise. When relevant, the policy receives a target state  $\mathbf{x}^*$  that should be achieved in the environment.

## 2.2 Control model

The control model is used to map observations to controls via a readout mechanism. We consider controllers that implement static policies, as conventionally used, as well as controllers that implement dynamic policies, where the control depends on a history of observations.

**Static policies** In case of static policies, we represent the policy as a function  $g$ , which computes the control signal with only the observations  $\mathbf{y}$  and potential target states  $\mathbf{x}^*$  as input. This setup matches related approaches for symbolic policy discovery [16, 24, 13] and is given by

$$u_j = g_j(\mathbf{y}, \mathbf{x}^*) \quad (3)$$

for  $1 \leq j \leq C$ .

**Dynamic policies** In case of dynamic policies, the policy becomes dependent on a dynamically evolving latent state, modeled by a system of ordinary differential equations, according to

$$\dot{\mathbf{a}}_i = f_i(\mathbf{a}, \mathbf{y}, \mathbf{u}, \mathbf{x}^*) \quad (4)$$

for  $1 \leq i \leq H$ . Note that the dynamic policies also receive the previous control as an additional input. The readout functions of the dynamic policies are similar to Equation 3, but the input to  $g_j$  is given by the latent state  $\mathbf{a}$  instead of the observations  $\mathbf{y}$ . That is,

$$u_j = g_j(\mathbf{a}, \mathbf{x}^*) \quad (5)$$

for  $1 \leq j \leq C$ .

## 2.3 Numerical integration

Both the dynamics of the environment and the controller are simulated as a coupled system over a specified time range  $[t_0, t_f]$  with  $t_0$  the initial time and  $t_f$  the final time. For the environment and dynamic policies, we need to resort to numerical integration. To this end, we make use of the Diffrax library [21]. Because the systems are stochastic, the integration is performed using the Euler-Heun method with a fixed step size  $\Delta t$  [22]. This results in trajectories  $\mathbf{x}_{0:f} = (\mathbf{x}_0, \dots, \mathbf{x}_f)$  and  $\mathbf{u}_{0:f} = (\mathbf{u}_0, \dots, \mathbf{u}_f)$  with  $\mathbf{x}_i$  and  $\mathbf{u}_i$  the state and control at time  $t_i$ . These trajectories are used to determine the policy's fitness using a fitness function  $F(\mathbf{x}_{0:f}, \mathbf{u}_{0:f})$ .

## 2.4 Genetic programming

The symbolic policies are evolved via genetic programming. This is achieved by representing the functions  $f_i$  and  $g_j$  as tree-structured computational graphs. GP is a variant of evolutionary algorithms that focuses on learning computer programs [23]. A population of solutions is evolved to satisfy a certain goal or task through stochastic optimisation. In GP, individuals are represented by a parse tree that is constructed from predefined sets of function nodes and leaf nodes. Function nodes cover mathematical operators and functions, while leaf nodes describe variables and constants. Individuals representing solutions that perform better will produce more offspring than individuals that have worse performance. GP is largely defined by two hyperparameters. The first hyperparameter is the number of generations, which determines how many iterations of evolution are performed. The second hyperparameter is the population size, which defines the number of candidates that are evolved at every generation. See Algorithm 1 (Appendix 2.4) for an overview of the GP algorithm. The GP algorithm consists of initialisation, evaluation and reproduction steps, as described in more detail in the following sections.

### 2.4.1 Initialisation

Initially the population consists of randomly generated individuals, which will generally score poorly on the problem. Nonetheless, the initial population can already have a large effect on the success of the full algorithm [5]. The initial population should cover enough of the search space for the genetic operations to be useful. The initialisation strategy that was originally introduced is called Ramped Half-and-Half [23]. In this method, trees are either sampled fully, where leaf nodes can only appear at the maximum depth, or the trees grow randomly, which means that leaf nodes can appear at earlier depths, so that the initial population covers both shallow and deep trees.

### 2.4.2 Evaluation

To evaluate an individual, its tree is transformed into a program of desired functionality and tested on a problem. The performance of the individual is expressed with a *fitness* score, computed with a fitness function. The fitness scores are used to select individuals for reproduction. After evaluation, parents are selected for reproduction using tournament selection [10].

### 2.4.3 Reproduction

In the GP, the new population is built with new candidate solutions that are obtained with crossover and mutation. In crossover the genotype of two individuals are combined to produce new trees. Fitter individuals are more likely to be selected for reproduction, therefore the offspring is built from promising tree structures. In both parents a random node from the tree is selected, after which these nodes and their subtrees are swapped. An example of the crossover operator is shown in Figure 1D. Uniform crossover is a variant of the standard crossover where multiple nodes can be swapped between a pair of trees without swapping full subtrees [35]. Uniform crossover improves the locality of the crossover operation, but both types of crossover can produce fit individuals and are therefore both included in our implementation.

Mutation was originally not integrated into GP [23], but mutation has shown to be a useful addition to the algorithm [27]. Mutation is applied to a single individual to generate one offspring and is applied instead of crossover in our implementation. Many aspects of trees can be mutated, for example changing, deleting or adding operators, replacing subtrees or changing variables or constants. Figure 1E shows an example of mutation, in which an operator is changed to a different type of operator. Besides crossover and mutation, the new population also consists of randomly generated individuals and the fittest individuals from the previous generation.

The number of trees that has to be optimised differs for the static and dynamic policies. The static policies should include a tree for every control input the problem requires. These trees also have to be evolved in the dynamic policies, but additional trees are optimised for every latent state variable. We chose to fix the size of the latent state in the dynamic policies and allow the readout function to learn how many latent states to use. To learn both a symbolic latent state and readout function simultaneously in the dynamic policies, the individuals in the GP algorithm are extended to learn multiple trees [8]. During reproduction, crossover and mutation are not applied to every tree in the individual to be able to make small jumps through the search space. Crossover is only applied to trees in the same position in two parents, and a third type of crossover is introduced in which only complete trees are swapped between individuals.

### 2.4.4 Regularisation

Regularisation is necessary in GP to produce interpretable trees and improve the efficiency of the optimisation. To regularise the size and complexity of the reproduced trees, a punishment relative to the number of nodes in a tree is added to the fitness [26]. Additionally, the depth of the trees is limited to seven, and during initialization the initial depth is set to four. To introduce more compact trees in the population, a small part of the population is simplified mathematically at every generation [18]. To improve diversity in the population during evolution, multiple subpopulations are evolved independently [11]. By configuring the hyperparameters in each subpopulation differently, exploration and exploitation is enforced explicitly [17]. Finally, dynamic policies with constant readout functions that only consist of targets or scalars and ignore the latent state often form local minima because they offer stable solutions. However such policies will never come close to high-performing policies. To improve the efficiency of the evolutionary search, every readout function of a dynamic policy that is reproduced or sampled will have at least one

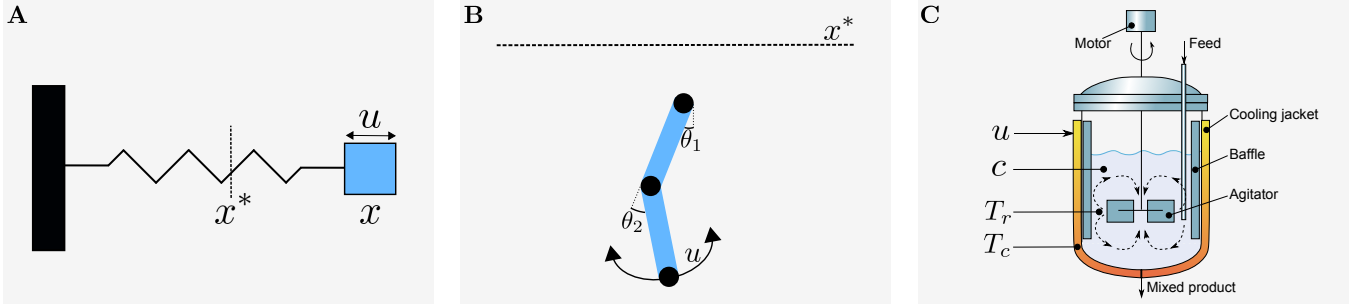


Figure 2: **Visualizations of the experiments.** (A) In the harmonic oscillator, the position of the oscillator  $x$  has to be moved to a target state  $x^*$  by applying the control force  $u$ . (B) The acrobot consists of two links, which are each defined by the angles  $\theta_1$  and  $\theta_2$ . To complete the swing up, the end of the second link has to be moved above the target height  $x^*$  by applying control force  $u$  on the second link. (C) The continuous stirred tank reactor is described by the concentration of reactant  $c$ , the temperature  $T_r$  in the main reactor, and the temperature  $T_c$  in the cooling jacket. The temperature in the reactor should be stabilised at a set point temperature  $T_r^*$ . The flow of coolant into the cooling jacket is controlled by  $u$ .

reference to a latent variable in its readout function to avoid such local minima, or else it is rejected for the next population.

## 2.5 Baselines

The symbolic policies generated with GP are compared with two baselines. The baselines are evaluated with the same population size and number of generations for every experiment.

The first baseline is random search of dynamic symbolic policies, which randomly samples a set of trees for each candidate, with candidates having the same model structure as the dynamic policies (Figure 1C). The random search policies have the same number of trees in the latent state and are built from the same set of functions and leaf nodes as used in GP. The maximum depth of trees found with random search is fixed to seven. Random search is included as a baseline to demonstrate if GP can find better solutions with less computation than random sampling, therefore showing the additional value of the genetic operators during optimisation.

To verify that the symbolic policies are high-performing, the symbolic policies are also compared to black-box policies modeled by neural differential equations (NDEs) [9]. The NDEs in our experiments implement Equations 4 and 5 using black-box neural networks. Specifically, we use

$$\dot{\mathbf{a}} = \tanh(\mathbf{A}\mathbf{z}) \quad (6)$$

with  $\mathbf{z} = (\mathbf{a}, \mathbf{y}, \mathbf{u}, \mathbf{x}^*, 1)$  a column vector concatenating the inputs and a constant, and  $\mathbf{A} \in \mathbb{R}^{N \times |\mathbf{z}|}$  a matrix. The linear readout layer is defined as

$$\mathbf{u} = \mathbf{B}\mathbf{v} \quad (7)$$

with  $\mathbf{v} = (\mathbf{a}, \mathbf{x}^*, 1)$  and  $\mathbf{B} \in \mathbb{R}^{C \times |\mathbf{v}|}$ . In this case, model parameters are optimised using covariance matrix adaption evolution strategies [14]. Evolutionary optimisation of weights in neural networks was shown to be a powerful alternative for gradient-based training in reinforcement learning tasks [33]. In all experiments, the dimension of  $\mathbf{a}$  was set to five for the NDE baseline. If policies discovered with GP can obtain similar fitness scores as the black-box NDE, the symbolic policies are said to be high-performing.

The performance of our method and the baselines is demonstrated through the best fitness at every generation during evolution, averaged over 20 independent evolutionary runs. The validation fitness of the best policy found in every run is displayed to confirm that the policies generalise to unseen conditions, but also to inspect the variance of convergence in the different evolutionary processes.

## 2.6 Environments

Our method and the baselines are evaluated on three different environments, as shown in Figure 2. The first environment is the stochastic harmonic oscillator, which is a linear environment that can be solved with a linear controller.

The policies are tested in a noisy setting, a partial observable setting where only a subset of the state variables is observed, and a setting where the environmental parameters vary. Here, an analytically optimal control policy, linear quadratic Gaussian (LQG) control, is used as an optimal baseline for comparison. The second environment is the acrobot swing up task with bounded continuous action space. This is a non-linear environment that requires a non-linear controller to perform the swing up. The policies solve the acrobot under noise and partial state observability, and in a third experiment the policies output two control signals. The third environment is the continuous stirred tank reactor (CSTR). The CSTR is a non-linear industrial system, which shows how well GP can find symbolic policies in more realistic settings. The parameters of the CSTR are varied in every trial. The chosen hyperparameter setting of the GP algorithm for each experiment are presented in Table 1 (Appendix 2.4). The choice of the function sets are described in the following subsections.

### 2.6.1 Stochastic harmonic oscillator

The stochastic harmonic oscillator (SHO) is a linear model that describes the position and velocity of an oscillating mass in a single dimension under random perturbations. The SHO is visualized in Figure 2A and the dynamics of the SHO are given by

$$d\mathbf{x} = (\mathbf{A}\mathbf{x} + \mathbf{b}u)dt + \mathbf{v}dw \quad (8)$$

with

$$\mathbf{A} = \begin{bmatrix} 0 & 1 \\ -\omega & -\zeta \end{bmatrix}, \quad \mathbf{b} = \begin{bmatrix} 0 \\ 1 \end{bmatrix}, \quad \mathbf{v} = \begin{bmatrix} 0 \\ 0.05 \end{bmatrix}. \quad (9)$$

Depending on the choice of  $\omega$  and  $\zeta$  we obtain different harmonic oscillators, reflecting different choices of the oscillator’s mass, spring constant and damping.

The fitness function was chosen as the negative quadratic cost function, defined as

$$F(\mathbf{x}_{0:f}, \mathbf{u}_{0:f}) = - \sum_{t=0}^f (\mathbf{x}_t - \mathbf{x}^*)^\top \mathbf{Q} (\mathbf{x}_t - \mathbf{x}^*) - r u_t^2 \quad (10)$$

with  $\mathbf{Q} = \text{diag}(0.5, 0)$  and  $r = 0.5$ . Here,  $\mathbf{Q}$  punishes the policy for the distance between  $\mathbf{x}$  and some target state  $\mathbf{x}^*$  whereas  $r$  penalizes the control strength. The initial condition  $\mathbf{x}_0$  is randomly sampled from a normal distribution with zero mean and variances 3 and 1 for the position and velocity respectively. The target position is chosen randomly by sampling uniformly between -3 and 3 in each trial, while the target velocity is always set to zero. As the optimal LQG control is linear, the function set includes basic arithmetic operators.

GP and the baselines are tested on the SHO in three different experiments. In the first experiment the policies interact with the standard setting of the SHO. In this experiment  $\mathbf{A}$  is specified with  $\omega = 1$  and  $\zeta = 0$  and the state observations are noisy. In the second experiment the state of the SHO is partially observed, as the policies only observe the position while the velocity is unknown.  $\mathbf{A}$  remains the same in this experiment. In the third experiment, the policies are evaluated on generalisability. In each trial  $\omega$  and  $\zeta$  are different, specifically  $\omega \sim U(0, 2)$  and  $\zeta \sim U(0, 1.5)$ . In this experiment both the position and velocity are observed again. The best dynamic symbolic policy found in the third experiment is also tested on SHO that change over time to analyse how well the latent states of the dynamic policy adapt to these changes. In the experiments with observation noise, the parameters of the readout function are set to  $\mathbf{D} = \mathbf{I}$  and  $\mathbf{\Sigma} = 0.3\mathbf{I}$  (see Equation 2). In experiments with partial state observability,  $\mathbf{D}$  is adapted such that only the relevant observations are returned and the dimension of  $\mathbf{\Sigma}$  is decreased to match the number of observations.

### 2.6.2 Acrobot swing up task

The acrobot is defined by two connected links with an angle  $\theta_i$  each, which is visualized in Figure 2B. The first link is connected to a fixed position. In the swing up task, the goal of the policy is to bring the end point of the second link above a certain threshold height. The dynamics of the acrobot are defined as follows [38]. Let  $\theta_1$  and  $\theta_2$  denote the angles of the first and second link, respectively. Their dynamics are given by

$$\begin{aligned} \ddot{\theta}_1 &= - \frac{d_2 \ddot{\theta}_2 + \phi_1}{d_1} \\ \ddot{\theta}_2 &= \frac{u_1 + d_1^{-1} d_2 \phi_1 - m_2 l_1 l c_2 \dot{\theta}_1^2 \sin(\theta_2) - \phi_2}{m_2 l_{c2}^2 + I_2 - d_1^{-1} d_2^2} \end{aligned}$$

with parameters as defined in Appendix B. In the acrobot experiment that requires two control forces, the state equation of  $\dot{\theta}_1$  is adapted to  $\dot{\theta}_1 = (u_2 - d_2 \dot{\theta}_2 - \phi_1)/d_1$ . In practice, we convert this system to a stochastic first-order system

$$d\mathbf{x} = f(\mathbf{x}, \mathbf{u})dt + \mathbf{V}d\mathbf{w}$$

with  $\mathbf{x} = (\theta_1, \theta_2, \dot{\theta}_1, \dot{\theta}_2)^\top$  where  $\mathbf{V} = \text{diag}(0, 0, 0.05, 0.05)$  adds noise to the angle accelerations.

The fitness function is a sparse reward function with control regularisation, defined as

$$F(\mathbf{x}_{0:f}, \mathbf{u}_{0:f}) = -t_f - \sum_{t=0}^f \mathbf{u}_t^\top \mathbf{R} \mathbf{u}_t \quad (11)$$

where  $t_f$  describes the time point at which the swing up is accomplished. The control  $\mathbf{u}$  is clipped between -1 and 1, forcing policies to learn to build momentum to accomplish the swing up. The swing up is accomplished when  $-\cos(\theta_1) - \cos(\theta_1 + \theta_2) > x^*$ , where  $x^*$  is a fixed target height in every trial. Hence, the policy must try to minimise  $t_f$  and its control use.

In every experiment,  $\mathbf{R} \in \mathbb{R}^{C \times C}$  is set to  $0.01\mathbf{I}$ ,  $x^*$  to 1.5 and the initial states are sampled from  $U(-0.1, 0.1)$ . Observations of  $\theta_i$  are wrapped between  $[-\pi, \pi]$  and a trial terminates when  $\dot{\theta}_1 > 8\pi$  or  $\dot{\theta}_2 > 18\pi$ . Policies are discovered to solve the acrobot in three different experiments. In the first experiment the state of the acrobot is observable with noise and control force is only applied to the second link. In the second experiment the acrobot state is made partially observable, as the policies no longer observe the angular velocities. As in the first experiment, the control force is only applied to the second link. The third experiment tests for scalability of the policies under noisy observations. The policies apply control forces to both links in this experiment, therefore the policy should return two outputs. To increase the memory capacity of the dynamic policies, the latent size in dynamic policies is increased to three. The observations of the acrobot include angles, therefore the sine and cosine functions are added to the function set of the GP algorithm, besides the arithmetic operators. As for the SHO, the parameters of the readout function are set to  $\mathbf{D} = \mathbf{I}$  and  $\mathbf{\Sigma} = 0.3\mathbf{I}$  in case of observation noise. In experiment with partial state observability,  $\mathbf{D}$  is again changed to exclude the unobserved variables and  $\mathbf{\Sigma}$  is shrunken to the correct dimension.

### 2.6.3 Continuous stirred tank reactor

The CSTR describes a chemical process following non-linear dynamics [40]. The CSTR consists of a main tank that contains a mixture of chemicals and a cooling jacket around the main tank. A visualization of the CSTR is presented in Figure 2C. To optimise the chemical process inside the main tank, the temperature has to be stabilised around a setpoint temperature. The temperature in the cooling jacket can be influenced directly by altering the input flow of coolant, which in turn affects the temperature in the main tank. The dynamics of the CSTR are defined as in [4], extended with a Wiener process to incorporate stochasticity. Let  $\mathbf{x} = (c, T_r, T_c)^\top$ . The CSTR defined as a stochastic first-order system

$$d\mathbf{x} = f(\mathbf{x}, \mathbf{u})dt + \mathbf{V}d\mathbf{w}$$

with  $\mathbf{V} = \text{diag}(0.025, 3, 3)$ . The state equation is defined as  $f(\mathbf{x}, \mathbf{u}) = [f_1(\mathbf{x}, \mathbf{u}), f_2(\mathbf{x}, \mathbf{u}), f_3(\mathbf{x}, \mathbf{u})]^\top$  with

$$\begin{aligned} f_1(\mathbf{x}, \mathbf{u}) &= \frac{q_r}{V_r} (c_f - c) + k(T_r)c \\ f_2(\mathbf{x}, \mathbf{u}) &= \frac{q_r}{V_r} (T_f - T_r) + \frac{-\Delta H}{\rho C_p} k(T_r)c + \frac{UA}{\rho C_p V_r} (T_c - T_r) \\ f_3(\mathbf{x}, \mathbf{u}) &= \frac{q_c}{V_c} (T_{cf} - T_c) + \frac{UA}{\rho C_p V_r} (T_r - T_c) \end{aligned}$$

and parameters as defined in Appendix C.

The fitness function is chosen as the negative quadratic cost function, defined as

$$F(\mathbf{x}_{0:f}, \mathbf{u}_{0:f}) = - \sum_{t=0}^f (\mathbf{x}_t - \mathbf{x}^*)^\top \mathbf{Q} (\mathbf{x}_t - \mathbf{x}^*) - r u_t^2 \quad (12)$$



where

$$\mathbf{Q} = \begin{bmatrix} 0 & 0 & 0 \\ 0 & 0.01 & 0 \\ 0 & 0 & 0 \end{bmatrix}, \quad r = 0.0001, \quad \mathbf{x}^* = \begin{bmatrix} 0 \\ T_r^* \\ 0 \end{bmatrix}. \quad (13)$$

The policy has to minimise the distance between the temperature in the reactor and the setpoint temperature  $T_r^*$ , while also minimising the control, i.e. the coolant flowrate. Only a single experiment is performed regarding the CSTR. This experiment tests policies for their generalisability to an industrial environment. The parameters of the CSTR are different in each trial, to simulate as if the policy is operating in multiple scenarios. In total, eight parameters vary between trials (Table 3 in Appendix C). Additionally, the concentration in the reactor is not observed, and the observations of the temperature in the reactor and cooling jacket are noisy. The function set of the GP algorithm is extended to include the exponential and logarithmic functions to aid expressions to deal with the values of the temperatures, which typically range between 200 and 600. The best dynamic symbolic policy evolved with GP is tested in a trial with changing setpoint temperatures, to analyse how the policy and latent state variables respond to these changes. To generate the observations,  $\mathbf{D}$  is defined such that the concentration is excluded from the observations and  $\Sigma = \text{diag}(7.5, 7.5)$ .

### 3 Results

We present a GP method for finding high-performing white-box symbolic policies for solving control problems. We consider both static and dynamic policies optimized by GP (GP-S and GP-D respectively), and test their performance by controlling three common control benchmark systems (as explained in detail in Section 2.6). We test whether GP evolves successful control policies for linear and non-linear environments, different observability levels, as well as changing environment conditions and multiple control dimensions. We compare the resulting control policies to those found from optimal control (where possible), random search (RS), and to a reference black-box model (NDEs).

#### 3.1 Genetic programming evolves linear and non-linear symbolic policies

To study whether GP is able to efficiently evolve symbolic policies we first consider a stochastic harmonic oscillator (SHO) with a static environment setting. For this particular control problem the optimal LQG controller gives us an upper bound on the fitness (Figure 3A, black curve). Given the simplicity of the control problem, even random search can find control policies with close to optimal performance (Figure 3A, gray dots). However, these policies can take a long time and many experiments to find (Figure 3A, purple curve), resulting in low consistency of the validation scores across different runs. Ideally, evolution should find such policies faster and more consistently. Indeed, using evolution strategies to optimise NDEs allows us to quickly find control policies close to optimal (Figure 3A, green curve).

To validate that GP can evolve symbolic policies that reach similar performance, we first optimized static symbolic policies (Figure 3A, blue curve). The initial average best fitness of GP-S is already close to the optimal fitness, which indicates that well-performing static policies already exist in the randomly sampled initial population, which is likely a result of the small search space of GP-S. However, from there on GP is not able to find policies reaching the optimal fitness, indicating that the forward policies do not have enough complexity to match the optimal controller. We next used GP to optimize dynamic symbolic policies (Figure 3A, orange curve). The average best fitness of GP-D begins significantly lower than GP-S does, reflecting the much larger search space and in turn lower probability to randomly sample a high-performing policy. However, from there on GP quickly converges to policies that are optimal or close to optimal, indicating that its internal dynamics are beneficial to deal with noisy observations. The GP-D solutions are also highly consistent across trials, although there was one outlier with less good performance (Figure 3A, blue dots).

The SHO can be stabilised with a linear controller, as can be deduced from the structure of the LQG controller. However, as most control problems require non-linear policies, it is important to demonstrate that such policies are also optimised with GP. Therefore, our method was applied to the acrobot swing-up task to demonstrate that non-linear policies are still evolved efficiently. Similarly to the previous experiment, random search performs much worse than the other methods in terms of average best fitness (Figure 3B, purple curve). The validation fitness is also worse, although there are some policies that overlap with the other methods (Figure 3B purple dots). NDE converges to a higher fitness than random search (Figure 3B, green curve), and the validation fitness of the best policies found with NDE is also better than any policy discovered with random search (Figure 3B, green dots).

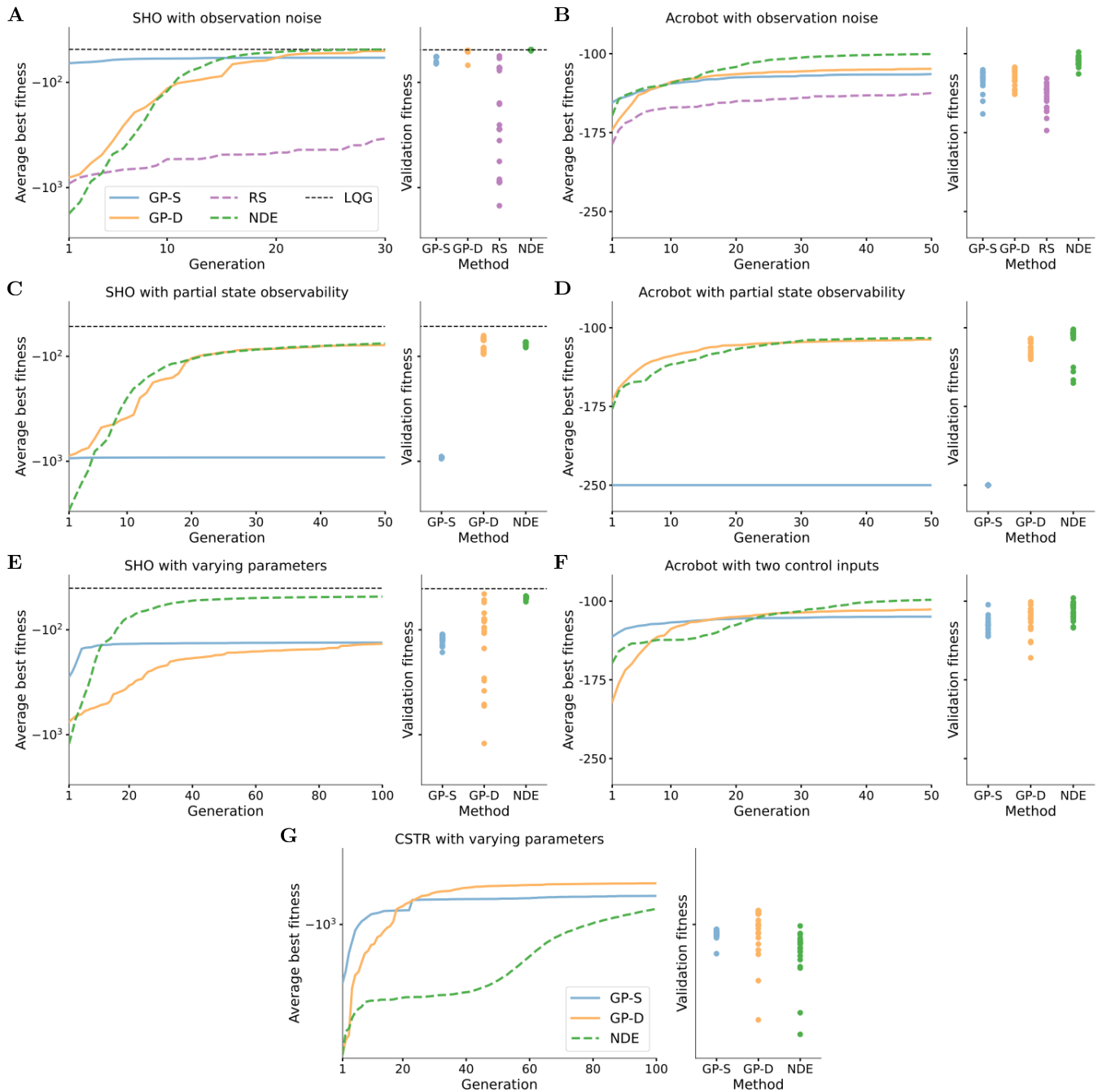


Figure 3: **Genetic programming evolves high-performing symbolic policies.** (A) Evolution results of stabilising the stochastic harmonic oscillator (SHO) in a target state. The left plot shows the best fitness at every generation during evolution, averaged over 20 independent runs. The methods included are genetic programming for static (GP-S) and dynamic (GP-D) policies, random search (RS) and neural differential equation (NDE). The LQG fitness is plotted as the analytical optimal fitness, averaged over 20 runs. The right plot presents the validation fitness obtained on unseen conditions with the best policy evolved in every evolutionary run. (B) Evolution results of the experiment on the acrobot under noisy observations. (C) Evolution results for the experiment in which the state of the SHO is partially observable. RS was excluded as it could not produce comparable results in panel A. (D) Evolution results of the experiment on the acrobot swingup under partial state observability. Again, RS was excluded as it could not produce comparable results in panel B. (E) Evolution results of the stabilisation of the SHO with varying parameters. (F) Evolution results for the acrobot swing up where control forces are applied to both links, which requires two-dimensional control outputs. (G) Evolution results of stabilising the CSTR to a setpoint temperature with varying parameters.

Static and dynamic symbolic policies were evolved with GP to analyse whether similar performance as the NDE can be obtained. GP-S converges at a fitness value higher than random search, but lower than the NDE (Figure 3B, blue curve). The average best fitness of GP-D is lower than GP-S initially, but converges to a slightly higher fitness during evolution (Figure 3B, orange curve). The validation fitness of the best policies evolved with GP-D (Figure 3B, orange dots) and GP-S (Figure 3B, blue dots) overlap largely.

Overall, the results in the experiment demonstrate that static and dynamic symbolic policies are effectively optimised with GP. Both high-performing linear and non-linear policies are evolved, therefore showing that GP is clearly advantageous for symbolic policy learning compared to random search. The black-box NDE is more consistent in finding high-performing policies, however the majority of the evolved symbolic policies are able to compete.

### 3.2 Dynamic symbolic policies remain robust under partial state observability

The previous experiments demonstrated that static and dynamic symbolic policies are successfully evolved for a linear and non-linear settings. However, these experiments assumed noisy observations of the full state, which is not representative for most real-life applications. We hypothesized that the memory capacity of the dynamic policies is particularly beneficial when the policies are confronted with partial observations of the state. To test this hypothesis, symbolic policies were evolved for stabilisation of the SHO and the acrobot swing-up under partial state observability, where the velocity is not observed in both environments.

The SHO environment remains linear, therefore optimal LQG controller again represents the upper bound fitness value (Figure 3C, black curve). Random search was excluded in this experiment, because it could not consistently discover high-performing policies in the previous experiment (Figure 3A, purple curve). The NDE converges to a slightly lower fitness (Figure 3C, green curve) than it did in the full observable SHO (Figure 3A, green curve). However, the NDE still consistently produced policies that are close to optimal in terms of performance.

As expected, the average best fitness of GP-S converges to a substantially poorer fitness than the NDE (Figure 3C, blue curve). The validation fitness of GP-S also shows that every policy obtains similar performance and fails to satisfy the task when the velocity is excluded from the observations (Figure 3C, blue dots). Differently from GP-S, well-performing dynamic symbolic policies are successfully optimised with GP in this experiment (Figure 3C, orange curve). The average best fitness of GP-D converges to a similar fitness as the NDE. Additionally, the validation fitness is consistent, and some policies even perform better than the NDE policies (Figure 3C, orange dots).

The dynamic symbolic policies perform significantly better than the static policies on the SHO with partial state observability. The acrobot swing-up experiment validates whether this difference in performance is also obtained in a non-linear environment. In this experiment, random search is again left out as baseline, because it could not produce comparable policies (Figure 3B, purple curve). The NDE approach converges to high-performing policies (Figure 3D, green curve), although at a slightly lower average best fitness than it did under full observability (Figure 3B, green curve). The validation fitness of the best NDE policies shows less consistency than in the previous experiments, as there are a few policies that perform substantially worse than the average (Figure 3D, green dots).

In the experiment with partial state observability in the SHO, the static policies failed to solve the task while the dynamic policies remained high-performing (Figure 3C). In the partially observable acrobot, similar findings are obtained. GP-S does not evolve a single policy that completes the swing up, as is observed from the constant fitness during evolution (Figure 3D, blue curve) and the lack of policies that obtain a validation fitness above the minimum fitness of 250 (Figure 3D, blue dots). The dynamic policies evolved with GP are able to solve the acrobot swing up (Figure 3D, orange curve). The validation fitness of GP-D shows consistency in performance among the discovered policies (Figure 3b, orange dots), even more so than the NDE baseline. The finding that dynamic symbolic policies are successful under partial observability was expected, because the best performing policy in the fully observable acrobot swing-up task did not include the velocity observations in its dynamics (Table 5, Acrobot, Observation noise).

The limited performance of the static symbolic policies under partial state observability compared to the dynamic symbolic policies and NDE can be contributed to the lack of memory in the static policies. The memory capacity in the dynamic policies allows for estimation of the velocity, which turns out to be crucial to solve the SHO and acrobot tasks successfully. The memory capacity in the dynamic symbolic policy significantly increases the search space, but enables the policies to satisfy its goals in environments with partial observability.

### 3.3 Symbolic policies generalise to varying environments

In realistic applications, policies will often be confronted with partial observations. However, the environment of interest might also differ between trials or change over time, therefore the policies have to be able to generalise to different environment specifics. To validate that generalising symbolic policies can be evolved, the policies have to stabilise the SHO of which the parameters vary in every trial.

For this experiment, the upper bound fitness is again obtained with the optimal LQG controller, which is computed independently for every parameter setting (Figure 3E, black curve). The average best fitness of the NDE approach converges close to the upper bound fitness (Figure 3E, green curve). The validation fitness of the NDE policies shows that the evolved policies are high-performing in each evolutionary run (Figure 3E, green dots).

To validate whether symbolic policies can generalise to varying environment settings, static policies are first evolved (Figure 3E, blue curve). The average best fitness during evolution of GP-S does not converge near the upper bound fitness and the fitness obtained by the NDE. The validation fitness of the best static policies shows that a ceiling has been reached, as every policy is located close to the average (Figure 3E, blue dots). The average best fitness of GP-D converges to a similar fitness as the GP-S (Figure 3E, orange curve). However, the validation fitness of the best dynamic symbolic policies shows an interesting pattern (Figure 3E, orange dots). Many of the dynamic symbolic policies obtain a validation fitness that is better than any static policy, and some even compare with NDE policies. On the other hand, in some evolution processes of dynamic symbolic policies, GP failed to discover well-performing dynamic policies, as is observed from the validation fitness that is lower than any validation fitness obtained by GP-S.

The inconsistency of the evolution of dynamic symbolic policies can be explained by the large search space. However, when dynamic policies are evolved successfully, they show to perform better than static policies are capable of. The memory capacity allows dynamic policies to discover useful properties about the environment that increase the generalisability compared to static policies. In our results, there are more evolutionary runs that result in dynamic policies that exceed the performance of static policies than the other way around. Therefore the addition of the memory capacity in symbolic policies proves to be more beneficial than it is disadvantageous. Nonetheless, the black-box NDE consistently produces policies that outperform most symbolic policies.

### 3.4 Genetic programming evolves higher-dimensional policies

As the search space of symbolic policies is large, especially for the dynamic symbolic policies, it is important to validate whether high-performing are optimised efficiently when the control dimension increases. In this experiment, the policies can apply control forces to both links to accomplish the acrobot swing-up. The NDE converges to a slightly higher fitness during evolution than in the other experiments on the acrobot, because more force can be applied to solve the swing up (Figure 3F, green curve). The best NDE policies obtain consistent validation fitness (Figure 3F, green dots).

Our method is first tested to produce static symbolic policies with two control outputs (Figure 3F, blue curve). The search space of static policies is still small compared to the dynamic policies, as is observed from the higher initial average best fitness compared to the other methods. The average best fitness of GP-S does not improve much during evolution, and converges at a worse fitness than the NDE. The validation fitness shows that most static policies perform similarly, but one evolved policy performs better than the other static policies (Figure 3F, blue dots). GP-D converges at a slightly better fitness than GP-S, but worse than NDE (Figure 3F, orange curve). The validation fitness obtained by dynamic symbolic policies mostly overlaps with that of the static symbolic policies and NDE policies, although a few policies are worse than any policy obtained by the other methods (Figure 3F, orange dots). This experiment demonstrates that GP still evolves higher-dimensional control policies that accomplish the acrobot swing up, even though the size of the search space increased even further.

### 3.5 Generalising symbolic policies are discovered for industrial application

In the final experiment, we apply our method to an industrial problem, the continuous stirred tank reactor (CSTR). A policy should stabilise the temperature in the reactor tank at a setpoint temperature, which is conducted by controlling the flow of coolant into the cooling jacket of the reactor. The goal of this experiment is to demonstrate that symbolic policies can be discovered that perform well in this realistic setting. The parameter setting in the CSTR is varied in each trial, therefore policies should generalise to different reactor specifics. GP is used to optimise static and dynamic policies again, and the policies are compared with NDE policies.

The average best fitness of the NDE policies has not converged yet after the dedicated number of generations, while being stuck at a poor fitness for the first half of the evolution (Figure 3G, green curve). A potential reason for the lower convergence efficiency of the NDE policies could be that they cannot easily approximate the non-linearity required to stabilise the reactor efficiently, which GP can do more easily, indicated by the faster convergence at a better fitness. The validation fitness of the NDE policies is lower on average than the symbolic policies, and contain a few bad-performing scores (Figure 3G, green dots).

GP-S converges to a lower fitness during evolution than NDE (Figure 3G, blue curve), and the validation fitness shows high consistency among the policies (Figure 3G, blue dots). GP-D obtains a better average best fitness as GP-S (Figure 3G, orange curve). GP-D discovered several policies that outperform GP-S and NDE in terms of validation fitness (Figure 3G, orange dots). However, the high-performing dynamic symbolic policies are again not consistently found, as some policies obtain a validation fitness significantly worse than any static policy.

The best static and dynamic policies are shown in Table 5 (CSTR, both Static and Dynamic). The evolved symbolic policies include non-linear terms such as exponentials and logarithms, but also multiplications of different variables. Such complex non-linear features are more difficult for the NDE to approximate, given the number of neurons in the latent state of the NDE. Increasing the number of neurons would improve its capability to approximate any function, however the optimisation of the network would become less efficient, requiring more computation power. GP can evolve these non-linear functionalities easily, which is yet another advantage of our method.

### 3.6 The latent states in a dynamic symbolic policy are transparent

The conducted experiments resulted in many diverse policies with interesting properties. The best validation fitness obtained with each method is presented in Table 4. Generally, the fitness score is the best for the NDE policies, but GP-D is often close and even outperforms NDE for some experiments. The best validation fitness of GP-D is higher than GP-S for every experiment. The corresponding static and dynamic symbolic policies are shown in Table 5. The mathematical expressions in the symbolic policies allow users to interpret a policy’s computations and actions. But in the case of dynamic symbolic policies, the latent states show transparent properties as well. These latent state variables can be plotted during a trial to analyse how the memory capacity is used to solve a problem. We analysed the best policies discovered in various experiments to investigate how these policies solve the task.

Firstly, we investigated the functionality of the best policy evolved to stabilise the SHO with varying parameters settings (Table 5, SHO, Varying parameters, Dynamic). Our interpretation of the symbolic expression of variable  $a_1$  in this policy is that it computes the distance between the target and position, adds the velocity and subtracts itself to decrease the influence of the noisy observations. Variable  $a_2$  integrates  $a_1$  multiplied with a constant, which we interpret as the an estimate of the cumulative error. The readout subtracts  $a_2$  and the cube of  $a_1$  from the target state to output the policy’s control.

By visualizing the latent states of the policy, we can analyse how the memory capacity aids to generalise to different environment settings. To demonstrate generalisability within a single trial, the policy was subjected to the SHO with parameters that change during the trajectory. When the parameters of the SHO change throughout the trajectory (Figure 4A, top row), the policy should continuously adjust its control signal to stabilise the SHO. The policy manages to keep the state close to the target state by increasing the strength of its negative control signal (Figure 4A, middle row). Variable  $a_1$  initially fluctuates until the position is stabilised close to the target, where after it stays close to 0 (Figure 4A, bottom row, blue curve). Variable  $a_2$  increases constantly over time to adjust to the changes in the environment, which causes the control force to increase (Figure 4A, bottom row, purple curve).

When the environment instantly changes (Figure 4B, top row), the policy adjusts accordingly and quickly stabilises the SHO in the target state again. Differently from Figure 4A, both latent state variables now react to the changes in the environment. Variable  $a_1$  responds with a small bump but stabilises again (Figure 4B, bottom row, blue curve). Initially, variable  $a_2$  stabilises once the SHO reaches its target state, but converges to a different value after the environment has changed to adjust the control to appropriate force (Figure 4B, bottom row, purple curve). In both scenarios, the policy robustly adjusts its control to the changes in the environment, and the response of the latent state to the changes is transparent.

When tested on the SHO the latent state of the policy is interpreted relatively easy, because the policy is (almost) fully linear. However, most problems require non-linear solutions. To still offer interpretability of a policy, the latent state should remain transparent when a policy becomes non-linear. To validate the transparency in non-linear policies, the best policy obtained from acrobot swing-up task under full observability is analysed (Table 5, Acrobot, Observation noise, Dynamic). Variable  $a_1$  computes the difference between the angles of the links. Variable  $a_2$  inputs

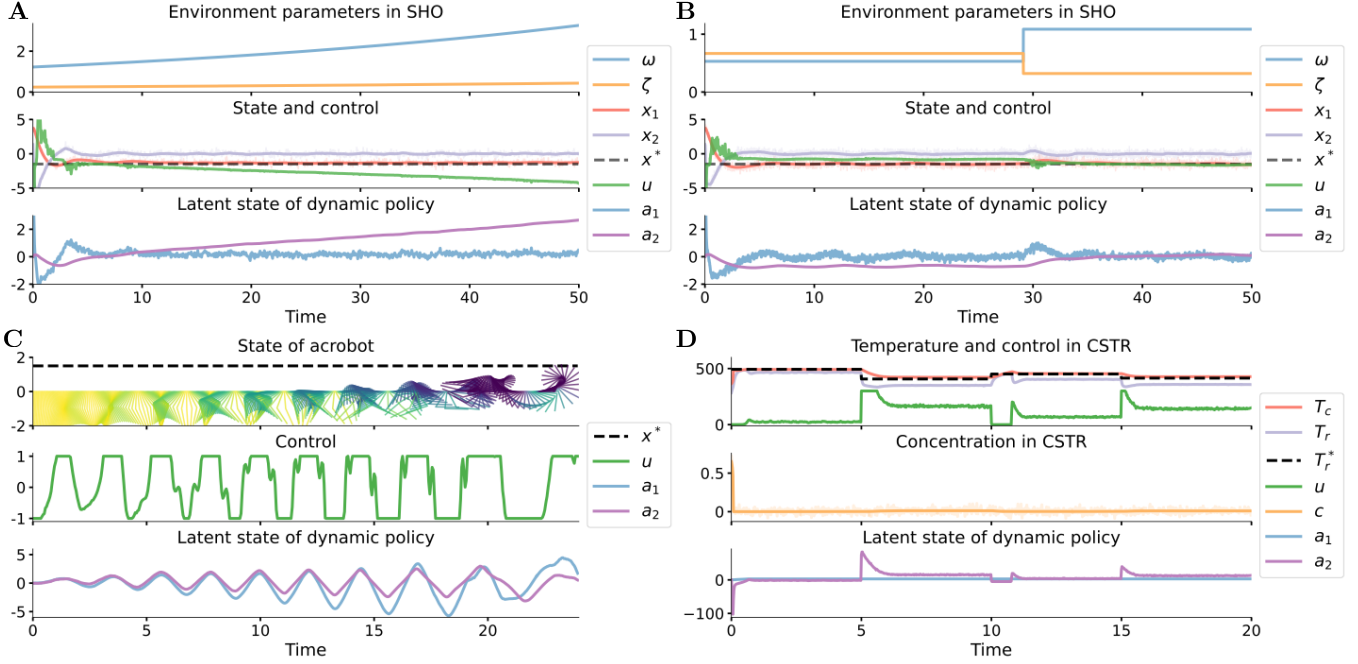


Figure 4: **Dynamic symbolic policies are transparent.** (A) Simulated trajectory of the stochastic harmonic oscillator (SHO) controlled by a dynamic symbolic policy. The parameters of the oscillator change over time, as is displayed in the top row. The plot in the second row shows the state and control in the trajectory. The shaded area around the states is observed by the policy. The latent state variables of the policy are presented in the bottom row. The policy used in this simulation is described in Table 5 (SHO, Varying parameters, Dynamic) (B) In this trajectory, the parameters in the SHO make a big jump at a random moment during the trial. The same policy is analysed as in panel A. (C) A simulated trajectory of the acrobot where control forces are applied to both links. The top row shows the position of the two links over time. The second row presents both control forces, and the bottom row shows only one of the latent state variables, because the other latent state variables are inactive. The policy is described in Table 5 (Acrobot, Two control inputs, Dynamic). (D) Simulated trajectory of the CSTR controlled with a policy evolved with GP. The top row shows the temperature of the reactor and cooling jacket when the policy controls the coolant inflow with varying setpoint temperatures. The second row presents the concentration of the reactant in the reactor. The bottom row shows the behavior of the latent state of the policy. The policy used in this simulation is described in Table 5 (CSTR, Dynamic).

the angle of the first link in two nested sine functions, multiplied with a scalar. The readout subtracts the cosine of  $a_1$  from  $a_2$ . Our interpretation of this policy is that it applies force in the direction of which the first link is compared to the centre point to build momentum on the first link, and increases the force when the two links are not closely aligned to add extra momentum to the second link, resembling a bang-bang controller.

The mathematical expressions of the non-linear policy to solve the acrobot are less straightforward to interpret than the linear policy that stabilises the SHO. Nonetheless, analysing the latent state of the non-linear policy could help with understanding the functioning of this policy. The policy accomplishes the swing up of the acrobot in a short time (Figure 4C, top row). The control force applied by the policy shows expected behaviour, switching between -1 and 1 to build momentum, and when the second link is close to the threshold the control force remains constant for longer (Figure 4C, middle row). The latents show similar patterns, although variable  $a_1$  fluctuates with a higher amplitude (Figure 4C, bottom row). The latent states are not as expressive as in the policy that was applied to the SHO, and it is difficult to understand the individual contribution of each variable. Nonetheless, there is still more transparency in these dynamics than would be the case in a black-box policy.

The previous experiments showed that the dynamic symbolic policies are transparent, but the problems of interest are simple control problems. For application purposes, it is more relevant if the policies remain interpretable in an industrial setting, such as the CSTR. The best policy discovered in the experiment conducted on the CSTR is tested

in a single trial to analyse the control and memory of the policy (Table 5 CSTR, Dynamic). We interpret the state equation of variable  $a_1$  as a scaling factor that converges to 2.92 during the trajectory. The state equation of variable  $a_2$  computes the error between the temperature and setpoint, and adds a self-connection to make the error estimate less affected by noise observations. The error estimate is scaled by the sum of the control,  $a_2$  itself and a constant. The readout scales  $a_2$  with the squared of  $a_1$ , and adds a multiplication of  $a_1$  with the logarithm of the setpoint temperature. The control therefore reacts to differences between the setpoint and current temperature, which is scaled by a factor that increases during the trajectory.

To increase the number of transparent responses in the trial, the setpoint temperature in the CSTR is changed several times during the trajectory. Therefore the policy has to adjust its control signal to change the temperature accordingly. The policy efficiently stabilises the temperature around each setpoint temperature (Figure 4D, top row). The control signal of the policy heavily changes when a new setpoint temperature is required, even remaining close to zero when the temperature has to increase. The concentration of the reactant in the main reactor goes to zero quickly and only slightly increases when the control input changes (Figure 4D, middle row). Variable  $a_1$  converges to 2.92 as expected (Figure 4D, bottom row, blue curve), while  $a_2$  shows a large response when the setpoint temperature changes. Together, the latent variables allow the policy to change its control output accordingly.

All these example trials demonstrate that the dynamic symbolic policies are not only interpretable, but also offer transparency in the latent states. The latents vary in their expressiveness, but overall analysing the latent state aids with understanding the functionality of a policy. The memory capacity already showed to be beneficial for increasing the robustness of a policy, however it also further improves the interpretability of symbolic policies.

## 4 Discussion

In this paper, we evolved white-box symbolic policies with genetic programming (GP) to solve control problems. The goal was to produce high-performing policies with interpretable dynamics. We considered two types of symbolic policies; static policies that are memory-less, and dynamic policies that have memory. The static policies include an expression for every control signal required, but the dynamic policies consist of a latent state and a readout function, for which individual trees were optimised with GP. We showed that GP was able to successfully evolve both static and dynamic symbolic policies for solving a variety of classic control problems. The dynamic policies allowed to perform successful control under noisy and partial state observations, as well as different and changing environments. We demonstrated the results in linear and a non-linear environment, and finally for an industrial environment. Overall, the results show that our method can optimise high-performing static and dynamic symbolic policies.

Currently, most approaches for discovering symbolic expressions with GP optimise single trees or apply tricks to evolve multiple trees independently. In the context of control, this would mean that only single dimensional control policies could be learned, resulting in purely static policies. By adding a latent state to the dynamic policies, the policies obtain memory capacity, by which we could improve their performance in dynamic environments. The latent state comes with the cost of requiring GP to optimise multiple trees together. In the experiments where the full state of the environment was observed, both the dynamic and static symbolic policies find policies that perform successfully. The search space of the dynamic policies is substantially larger, as is observed from the poor initial fitness compared to the initial fitness of the static policies and the fewer generations the static approach needs to converge. The validation fitness of the best static policies evolved in each run shows that these policies consistently converge to a similar expression and score. The validation fitness of the dynamic policies displays a larger spread, indicating that the evolution does not consistently result in policies of similar quality. The inconsistency in evolution can also be explained by the significantly larger search space of the dynamic policies.

The larger search space and consequently less consistent optimisation is a disadvantage of the addition of a latent state to the policies. However, the experiments with partial state observability show that the latent state also significantly improves the robustness of the policies. Static policies are unable to solve the tasks when the observations are incomplete, while the dynamic policies achieve similar performance as in the experiments with observation noise only. In environments with full state observability, our method discovers multiple policies that are better than any static policy, although these policies are not found consistently. Overall, our method evolves dynamic symbolic policies efficiently given the large search space, and the resulting policies are generally better than the static policies.

One way to improve the consistency and convergence rate of the evolution of dynamic symbolic policies would be to increase computational power. The hyperparameters of GP that relate to the computation power are the population

size and number of generations. These hyperparameters were chosen to be similar to values commonly used in literature to demonstrate that our method evolves these policies relatively efficiently. Nonetheless the convergence rate of our method could be improved by increasing these hyperparameters, which should increase the chance of evolving policies that compete with the black-box baseline.

The black-box method that was used for comparison is a neural differential equation optimised with covariance-matrix adaptation evolution strategies, as this approach has been proven to be powerful alternative to gradient descent optimisation in reinforcement learning settings [33]. The results demonstrate that symbolic policies are evolved that generally obtain comparable performance as the black-box baseline. The black-box baseline does have more consistent performance, but the white-box policies have several other advantages over the black-box policies. The main advantage of the symbolic policies is that the expressions of the white-box policies are interpretable and can be analysed to gain new insights. Additionally, the behaviour of the latent states is transparent, as demonstrated in Figure 4. This focus on interpretable policies relates to the field of scientific machine learning [30]. In scientific machine learning, knowledge and insights about data is sought with data-driven approaches. Since the latent and readout functions in our method were not directed to learn specific properties, the policies could discover different interesting features from scratch in every evolutionary run. Examples of learned properties are error estimates, reliable estimates of noisy observations, features from the environment and bang-bang control (Table 5).

While results are promising, there is room for future improvement of our method for evolving dynamic symbolic policies, both in terms of performance of the discovered policies and the efficiency of the search algorithm. GP in general is inefficient for optimisation of constants, because the search space is extremely large. Hybrid GP is an extension that combines standard GP with numerical optimisation, such as gradient-based methods or evolution strategies [39]. Focused optimisation of the constants improves the performance of the policy, but it could also save time during the search process of GP. Hybrid GP either optimises the constants of the final policy, or constant optimisation is integrated in the evolution progress itself, as was done in [8].

Another improvement would be to vary the number of latent states through evolution as well, similar to the NEAT algorithm [36]. With GP the size of the latent state in a policy can be increased when more memory capacity is beneficial to solve a problem. Similarly the number of latents can be decreased when not all memory capacity is necessary to solve a problem. The search space grows even more with this implementation, however the policies will consist only of relevant trees. Besides the described options there are many improvements for more efficient optimisation in GP, such as semantic reproduction [41], population diversity control [7] and self-adaptation of hyperparameters [2].

Note that we chose to learn symbolic expressions for both the latent state and readout functions. To further increase the interpretability in the discovered policies, the readout could be learned as a vector that is multiplied with the latent state to produce a control signal. This way, all non-linear functionality is evolved in the latent state, and the relation between the latent state and control signal becomes easier to understand. The robustness of evolution also improves, as less trees have to be optimised with GP, although another method for optimising the readout vector should be introduced.

The memory in dynamic policies demonstrated to improve the generalisability to different parameter settings in an environment. However, this could be further extended to evolve a single policy that can solve different control problems, which relates to meta-learning. In [20], genetic programming is used to construct a memory-based agent that solves six different control problems under partial state observability, which has to recognize the task at hand purely from the observations. Our work could be integrated to replace the model of the agent with a dynamic symbolic policy. The interpretable policy expression and transparent latent state would aid in understanding how the agent solves different tasks with the same policy.

Lastly, a major limitation of GP, which holds especially for the dynamic policies, is the huge search space. Our method showed to be scalable when the environment required two control outputs. Nonetheless, it is important to test our method on problems that receive higher-dimensional control and more observations, such as robot control. Future work would be to extend our research to high-dimensional problems, and to analyse how the GP algorithm should be improved to deal with the increased search space efficiently.

We conclude that the use of genetic programming is a viable route towards learning interpretable, efficient and general dynamic symbolic policies for control. We hope that this adds an important tool to the practitioners' toolbox in the endeavour to create trustworthy AI systems.



## Acknowledgements

This publication is part of the project ROBUST: Trustworthy AI-based Systems for Sustainable Growth with project number KICH3.L TP.20.006, which is (partly) financed by the Dutch Research Council (NWO), ASMPPT, and the Dutch Ministry of Economic Affairs and Climate Policy (EZK) under the program LTP KIC 2020-2023. All content represents the opinion of the authors, which is not necessarily shared or endorsed by their respective employers and/or sponsors.

## References

- [1] Amina Adadi and Mohammed Berrada. “Peeking inside the black-box: a survey on explainable artificial intelligence (XAI)”. In: *IEEE Access* 6 (2018), pp. 52138–52160.
- [2] Peter J Angeline. “Two self-adaptive crossover operators for genetic programming”. In: *Advances in Genetic Programming* (1996), pp. 89–109.
- [3] Anuradha M Annaswamy, Karl H Johansson, and George J Pappas. “2030 Control for Societal-Scale Challenges: Road Map”. In: *IEEE Control Systems Society* (2023).
- [4] Rita Antonelli and Alessandro Astolfi. “Continuous stirred tank reactors: easy to stabilise?”. In: *Automatica* 39.10 (2003), pp. 1817–1827.
- [5] Lawrence Beadle and Colin G Johnson. “Semantic analysis of program initialisation in genetic programming”. In: *Genetic Programming and Evolvable Machines* 10 (2009), pp. 307–337.
- [6] Josh Bongard and Hod Lipson. “Automated reverse engineering of nonlinear dynamical systems”. In: *Proceedings of the National Academy of Sciences* 104.24 (2007), pp. 9943–9948.
- [7] Edmund K Burke, Steven Gustafson, and Graham Kendall. “Diversity in genetic programming: An analysis of measures and correlation with fitness”. In: *IEEE Transactions on Evolutionary Computation* 8.1 (2004), pp. 47–62.
- [8] Hongqing Cao et al. “Evolutionary modeling of systems of ordinary differential equations with genetic programming”. In: *Genetic Programming and Evolvable Machines* 1 (2000), pp. 309–337.
- [9] Ricky TQ Chen et al. “Neural ordinary differential equations”. In: *Advances in Neural Information Processing Systems* 31 (2018).
- [10] Yongsheng Fang and Jun Li. “A review of tournament selection in genetic programming”. In: *International Symposium on Intelligence Computation and Applications*. Springer. 2010, pp. 181–192.
- [11] Francisco Fernandez, Marco Tomassini, and Leonardo Vanneschi. “An empirical study of multipopulation genetic programming”. In: *Genetic Programming and Evolvable Machines* 4 (2003), pp. 21–51.
- [12] Jianping Gou et al. “Knowledge distillation: A survey”. In: *International Journal of Computer Vision* 129.6 (2021), pp. 1789–1819.
- [13] Jiaming Guo et al. “Efficient Symbolic Policy Learning with Differentiable Symbolic Expression”. In: *Advances in Neural Information Processing Systems* 36 (2024).
- [14] Nikolaus Hansen. “The CMA evolution strategy: A tutorial”. In: *arXiv preprint arXiv:1604.00772* (2016).
- [15] Nicolas Heess et al. “Memory-based control with recurrent neural networks”. In: *arXiv preprint arXiv:1512.04455* (2015).
- [16] Daniel Hein, Steffen Udluft, and Thomas A Runkler. “Interpretable policies for reinforcement learning by genetic programming”. In: *Engineering Applications of Artificial Intelligence* 76 (2018), pp. 158–169.
- [17] Francisco Herrera and Manuel Lozano. “Gradual distributed real-coded genetic algorithms”. In: *IEEE transactions on Evolutionary Computation* 4.1 (2000), pp. 43–63.
- [18] Dale C Hooper and Nicholas S Flann. “Improving the accuracy and robustness of genetic programming through expression simplification”. In: *Proceedings of the 1st Annual Conference on Genetic Programming*. 1996, pp. 428–428.

- [19] Hitoshi Iba. “Inference of differential equation models by genetic programming”. In: *Information Sciences* 178.23 (2008), pp. 4453–4468.
- [20] Stephen Kelly et al. “Evolving hierarchical memory-prediction machines in multi-task reinforcement learning”. In: *Genetic Programming and Evolvable Machines* 22 (2021), pp. 573–605.
- [21] Patrick Kidger. “On Neural Differential Equations”. PhD thesis. University of Oxford, 2021.
- [22] P.E. Kloeden, E. Platen, and H. Schurz. *Numerical Solution of SDE through Computer Experiments*. Springer, 1994.
- [23] John R Koza. “Genetic programming as a means for programming computers by natural selection”. In: *Statistics and Computing* 4 (1994), pp. 87–112.
- [24] Mikel Landajuela et al. “Discovering symbolic policies with deep reinforcement learning”. In: *International Conference on Machine Learning*. PMLR. 2021, pp. 5979–5989.
- [25] Octavio Loyola-Gonzalez. “Black-box vs. white-box: Understanding their advantages and weaknesses from a practical point of view”. In: *IEEE Access* 7 (2019), pp. 154096–154113.
- [26] Sean Luke and Liviu Panait. “A comparison of bloat control methods for genetic programming”. In: *Evolutionary Computation* 14.3 (2006), pp. 309–344.
- [27] Sean Luke and Lee Spector. “A comparison of crossover and mutation in genetic programming”. In: *Genetic Programming* 97 (1997), pp. 240–248.
- [28] Erika Puiutta and Eric MSP Veith. “Explainable reinforcement learning: A survey”. In: *International Cross-Domain Conference for Machine Learning and Knowledge Extraction*. Springer. 2020, pp. 77–95.
- [29] Markus Quade et al. “Prediction of dynamical systems by symbolic regression”. In: *Physical Review E* 94.1 (2016), p. 012214.
- [30] Christopher Rackauckas et al. “Universal differential equations for scientific machine learning”. In: *arXiv preprint arXiv:2001.04385* (2020).
- [31] Gabrielle Ras et al. “Explainable deep learning: A field guide for the uninitiated”. In: *Journal of Artificial Intelligence Research* 73 (2022), pp. 329–396.
- [32] Erina Sakamoto and Hitoshi Iba. “Inferring a system of differential equations for a gene regulatory network by using genetic programming”. In: *Proceedings of the 2001 Congress on Evolutionary Computation (IEEE Cat. No. 01TH8546)*. Vol. 1. IEEE. 2001, pp. 720–726.
- [33] Tim Salimans et al. “Evolution strategies as a scalable alternative to reinforcement learning”. In: *arXiv preprint arXiv:1703.03864* (2017).
- [34] Michael Schmidt and Hod Lipson. “Distilling free-form natural laws from experimental data”. In: *Science* 324.5923 (2009), pp. 81–85.
- [35] William M Spears and Vic Anand. “A study of crossover operators in genetic programming”. In: *International Symposium on Methodologies for Intelligent Systems*. Springer. 1991, pp. 409–418.
- [36] Kenneth O Stanley and Risto Miikkulainen. “Evolving neural networks through augmenting topologies”. In: *Evolutionary Computation* 10.2 (2002), pp. 99–127.
- [37] Felipe Petroski Such et al. “Deep neuroevolution: Genetic algorithms are a competitive alternative for training deep neural networks for reinforcement learning”. In: *arXiv preprint arXiv:1712.06567* (2017).
- [38] Richard S Sutton. “Generalization in reinforcement learning: Successful examples using sparse coarse coding”. In: *Advances in Neural Information Processing Systems* 8 (1995).
- [39] Alexander Topchy, William F Punch, et al. “Faster genetic programming based on local gradient search of numeric leaf values”. In: *Proceedings of the Genetic and Evolutionary Computation Conference (GECCO-2001)*. Vol. 155162. Morgan Kaufmann San Francisco, CA. 2001.
- [40] Ashok Uppal, Willis Harmon Ray, and Aubrey B Poore. “On the dynamic behavior of continuous stirred tank reactors”. In: *Chemical Engineering Science* 29.4 (1974), pp. 967–985.
- [41] Leonardo Vanneschi, Mauro Castelli, and Sara Silva. “A survey of semantic methods in genetic programming”. In: *Genetic Programming and Evolvable Machines* 15 (2014), pp. 195–214.

- [42] Yu Zhang et al. “A survey on neural network interpretability”. In: *IEEE Transactions on Emerging Topics in Computational Intelligence* 5.5 (2021), pp. 726–742.

# Appendices

## A Genetic programming

Our implementation of genetic programming followed Algorithm 1. The hyperparameters and function sets we used in each experiment are presented in Table 1. The choice for the population size and number of generations (see Section 2.4) were chosen to balance efficiency and consistent convergence empirically. The elite percentage was set to 0.1 in every experiment. The choice of the function sets are explained in the corresponding environment sections.

---

### Algorithm 1 Genetic programming algorithm

---

**Input** Number of generations  $G$ , population size  $N$ , elite percentage  $E$ , fitness function  $F$

- 1: *initialise* population  $P$  with size  $N$  (Section 2.4.1)
  - 2: **for**  $g$  in  $G$  **do**
  - 3:   *evaluate* each individual in  $P$  on  $F$  (Section 2.4.2)
  - 4:   offspring  $O \leftarrow \{\}$
  - 5:   append fittest  $E$  of  $P$  to  $O$
  - 6:   **while**  $\text{size}(O) < N$  **do**
  - 7:     randomly select *reproduce* from {crossover, mutation, simplification, sample}
  - 8:     randomly select parents  $p$  from  $P$  with tournament selection
  - 9:     children  $c = \text{reproduce}(p)$  (Section 2.4.3)
  - 10:    append  $c$  to  $O$
  - 11:   **end while**
  - 12:    $P \leftarrow O$
  - 13: **end for**
  - 14: **return** fittest individual in  $P$
- 

Table 1: Hyperparameters of the genetic programming algorithm used in every experiment.

Hyperparameter	SHO			Acrobot			CSTR
	Exp 1	Exp 2	Exp 3	Exp 1	Exp 2	Exp 3	Exp 1
Population Size	500	500	1000	500	500	1000	1000
Number of Generations	30	50	100	50	50	50	100
Latent state size	2	2	2	2	2	3	2
Function set	+, -, *, /, power			+, -, *, /, power, sin, cos			+, -, *, /, power, exp, log

## B Acrobot parameters

The acrobot dynamics are defined in terms of the variables

$$\begin{aligned}
 d_1 &= m_1 l_{c1}^2 + m_2 (l_1^2 + l_{c2}^2 + 2l_1 l_{c2} \cos(\theta_2)) + I_1 + I_2 \\
 d_2 &= m_2 (l_{c2}^2 + l_1 l_{c2} \cos(\theta_2)) + I_2 \\
 \phi_1 &= -m_2 l_1 l_{c2} \dot{\theta}_2^2 \cos(\theta_2) - 2m_2 l_1 l_{c2} \dot{\theta}_2 \dot{\theta}_1 \sin(\theta_2) + (m_1 l_{c1} + m_2 l_1) g \cos\left(\theta_1 - \frac{\pi}{2}\right) + \phi_2 \\
 \phi_2 &= m_2 l_{c2} g \cos\left(\theta_1 + \theta_2 - \frac{\pi}{2}\right).
 \end{aligned}$$

with parameters of the system as shown in Table 2.

Table 2: Parameters of the acrobot swing up task.

Parameter	Unit	Description	Value or Range
$\theta_i$	rad	Angle of a link	$\theta_i(0) \sim U(-0.1, 0.1)$
$\dot{\theta}_i$	rad/s	Angular velocity of a link	$\dot{\theta}_i(0) \sim U(-0.1, 0.1)$
$l_i$	m	Length of a link	1.0
$m_i$	kg	Mass of a link	1.0
$l_{ci}$	m	Position of the center of mass of a link	0.5
$I_i$	kg m <sup>2</sup>	Moment of inertia of a link	1.0
$g$	m/s <sup>2</sup>	Gravity	9.81

## C Continuous stirred tank reactor parameters

The descriptions of each parameter in the CSTR dynamics are shown in Table 3. Table 3 also contains the value, initial condition or sample range for each parameter. The variables that are indicated with a range are uniformly sampled within this range in every trajectory. The initial conditions of  $c$ ,  $T_r$  and  $T_c$  are uniformly sampled from the given distribution. The controlled parameter is clipped between 0 and 300. The reaction rate is defined as  $k(T_r) = k_0 \exp(-E/RT_r)$ .

Table 3: Parameters of the continuous stirred tank reactor. Each parameter is either set to a value, a function or sampled uniformly given a range.

Parameter	Unit	Description	Value or Range
$c$	gmol/liter	Reactant concentration	$c(0) \sim U(0.5, 1.0)$
$T_r$	K	Reactor temperature	$T(0) \sim U(350, 375)$
$T_c$	K	Cooling jacket temperature	$T_c(0) \sim U(275, 300)$
$T_r^*$	K	Setpoint temperature	{400, 500}
$q_r$	liters/min	Feed flowrate of reactant into reactor	{75, 125}
$q_c$	liters/min	Feed flowrate of coolant into cooling jacket	Controlled parameter
$c_f$	gmol/liters	Feed concentration of reactant into reactor	1
$T_f$	K	Feed temperature of reactant into reactor	{300, 350}
$T_{cf}$	K	Feed temperature of coolant into cooling jacket	{250, 300}
$V_r$	liters	Volume of reactor	{75, 150}
$V_c$	liters	Volume of cooling jacket	{10, 30}
$\Delta H$	J/gmol	Enthalpy of reaction	{-55000, -45000}
$\rho$	g/liters	Density	1000
$C_p$	J/g/K	Heat capacity	{0.2, 0.35}
$UA$	J/min/K	Heat transfer coefficient	{25000, 75000}
$k_0$	1/min	Arrhenius pre-exponential	$7.2 \cdot 10^{10}$
$E$	J/gmol	Activation energy	72750
$R$	J/gmol/K	Gas constant	8.314
$k(T_r)$	1/min	Reaction rate	Function of temperature

## D Discovered policies

Table 4 shows the best validation fitness per experiment obtained by static symbolic policies (GP-S), dynamic symbolic policies (GP-D), and the two baselines; random search (RS) and the black-box neural different equations (NDE). GP-D outperforms GP-S in every experiment, and sometimes even outperforms NDE. The corresponding best static and dynamic symbolic policies discovered in each experiment are presented in Table 5. The static policies contain as many expressions as the environment has inputs. The dynamic policies contain another set of expressions for the state equations of the latent state.

Table 4: Best fitness of each method on the validation set in each experiment. The methods include random search (RS), neural differential equation (NDE) and genetic programming of static (GP-S) and dynamic (GP-D) policies. RS was only included in the experiments with full observability, and excluded from the others as it did not produce competitive results. The bold fitness indicates it is the best for an experiment. For all experiments, the dynamic symbolic policy outperforms the static symbolic policy.

Experiment	RS	NDE	GP-S	GP-D
Harmonic oscillator (Observation noise)	-56.11	<b>-48.85</b>	-57.28	-49.66
Harmonic oscillator (Partial state observability)	-	-72.76	-903.44	<b>-63.35</b>
Harmonic oscillator (Varying parameters)	-	-47.76	-110.25	<b>-45.56</b>
Acrobot (Observation noise)	-123.64	<b>-98.45</b>	-115.31	-112.82
Acrobot (Partial state observability)	-	<b>-101.47</b>	-250.0	-110.23
Acrobot (Two control inputs)	-	<b>-97.02</b>	-103.43	-100.69
CSTR	-	-1017.72	-1059.31	<b>-845.33</b>

Table 5: Best static and dynamic policies discovered with genetic programming for every experiment.  $u$  represents the function that outputs the control signal. In the dynamic policies, the functions of  $a_i$  represent the state equations of the latent state variables. When a latent variable is not referred to in any of the other expressions, it is labelled as inactive.

Experiment	Static	Dynamic
SHO Observation noise	$u = -0.61 y_2 + x^*$	$u = -2 a_1 + 2.60 a_2 + x^*$ $\dot{a}_1 = y_2$ $\dot{a}_2 = -u + x^*$
SHO Partial state observability	$u = 0.75 x^* - 0.11$	$u = 0.45 (a_1 + x^*)$ $\dot{a}_1 = 2 a_2 - u + x^*$ $\dot{a}_2 = -a_2 - 0.99 u + y_1$
SHO Varying parameters	$u = -1.10 y_1 - 0.73 y_2 + 1.83 x^* + 0.17$	$u = -a_1^3 - a_2 + x^*$ $\dot{a}_1 = 27.76 (-a_1 + y_1 + y_2 - x^*)$ $\dot{a}_2 = 0.32 a_1$
Acrobot Observation noise	$u = -y_3 + 1.29 \sin(y_4)$	$u = 2 a_2 - \cos(2 a_1)$ $\dot{a}_1 = 2 y_1 - 2 y_2$ $\dot{a}_2 = 5.47 \sin(\sin(y_1))$
Acrobot Partial state observability	No successful policies	$u = 1.87 a_1 + \cos(a_2)$ $\dot{a}_1 = 2.06 y_1$ $\dot{a}_2 = y_1 - 2.68$
Acrobot Two control inputs	$u_1 = 0.64 y_4 + \sin(y_4) - 0.04$ $u_2 = \sin(0.37 y_3)$	$u_1 = 2.71 \cos(a_2 - 0.57)$ $u_2 = -a_2 - 1.48$ $\dot{a}_1 = -8.66 a_1 + y_4$ (inactive) $\dot{a}_2 = -3.44 y_2$ $\dot{a}_3 = y_3$ (inactive)
CSTR	$u = T_c^4 (T_r^*)^{-3} - T_r$	$u = a_1^2 a_2 + 2 a_1 \log(T_r^*)$ $\dot{a}_1 = (2.92 - a_1)(u_1 + 2.98)$ $\dot{a}_2 = (u_1 - a_2 + 2.37)(a_2 - T_r^* + T_r)$